Supporting Information

Citrate Coordination and Bridging of Gold Nanoparticles: The Role of Gold Adatoms in AuNP Ageing

*David-Benjamin Grys†, Bart de Nijs†, Andrew R. Salmon†, Junyang Huang†, Wenting Wang†, Wei-Hsin Chen†, Oren A. Scherman‡, Jeremy J. Baumberg†**

† NanoPhotonics Centre, Cavendish Laboratory, Department of Physics, JJ Thompson Avenue, University of Cambridge, Cambridge, CB3 0HE, UK

‡ Melville Laboratory for Polymer Synthesis, Department of Chemistry, University of Cambridge, Lensfield Road, Cambridge CB2 1EW, UK

Characterisation of stock AuNP suspension. The AuNPs were synthesised according to the standard Turkevich/Frens protocol (see experimental section). To investigate the influence of cations on AuNP 'ageing', two batches of AuNPs based on trisodium citrate TSC or tripotassium citrate TPS were made. The UV-vis spectra (Figure **S1a**) and zeta size measurements (Figure **S1c**) suggest that the AuNP concentration, size and size distribution are near-identical.

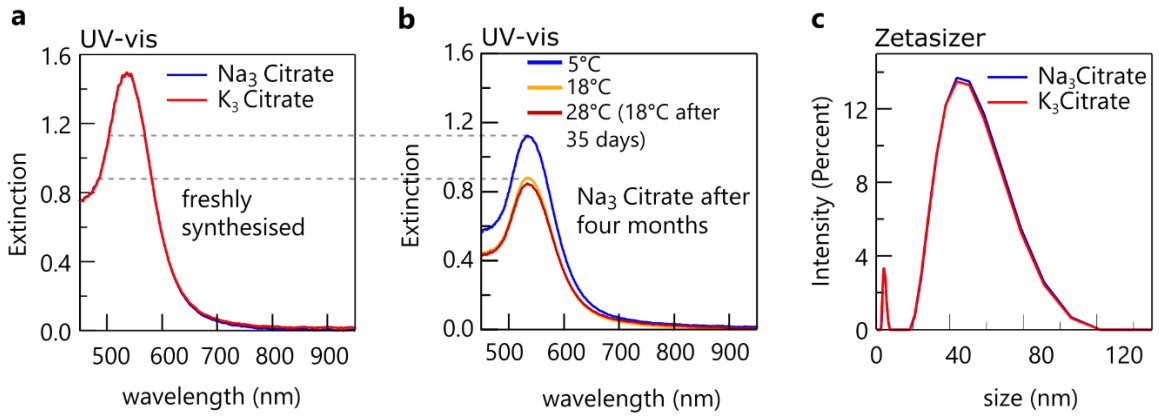

Figure S1. Characterisation of in-house AuNPs. (a) UV-vis spectra showing similar optical densities between trisodium and tripotassium citrate AuNPs. (b) UV-vis spectra showing optical densities after four months. (c) Zetasize measurements confirm that the K_3 and Na_3 have almost the same size and also size distribution.

Since the gold chloride to citrate ratio of 1:1.33 was the same for both batches, this also means that K^+ and Na^+ have no influence on the reaction kinetics. The hydrodynamic diameter is ~49.7 nm with a standard deviation of ~17.6 nm. The pH of the freshly synthesised AuNP suspension is 3.5±0.1 as a result of the citrate to $HAuCl_4$ ratio. The low pH is advantageous to keep citrate break-down products off the gold surfaces. With pKa=4.7[1], acetate/acetic acid (the final by-product) will be fully protonated. Despite the low pH, the AuNPs are stable for months. Even after four months from the day of synthesis, no signs of aggregation are observed in the UV-vis spectra (Figure **S1c**). The decrease in optical densities is caused by AuNPs deposited on the inside walls of the centrifuge tubes used to store the AuNP suspensions. During the ageing experiments, no deposition was noticed on the walls of the containers.

Ageing experiment for higher pH values and salted AuNPs. The ageing experiment was repeated by "salting" the AuNPs with trisodium citrate (TSC) and sodium chloride (NaCl) instead of using CB[5] as the nano-spacer.

This is to rule out potential interference between CB[5] and citrate during the ageing process and to determine the coordination modes of citrate. The spectra of fresh and aged AuNPs contain peaks which are also present in the ageing experiments with CB[5] (Figure **S2a**,**b**). To observe and compare ageing at different protonation states of citrate, the pH values of the AuNP suspensions are adjusted to 3.8, 5.5 and 6.8 by adding citrate buffer (TSC/citric acid) with a final concentration of 5 mM.

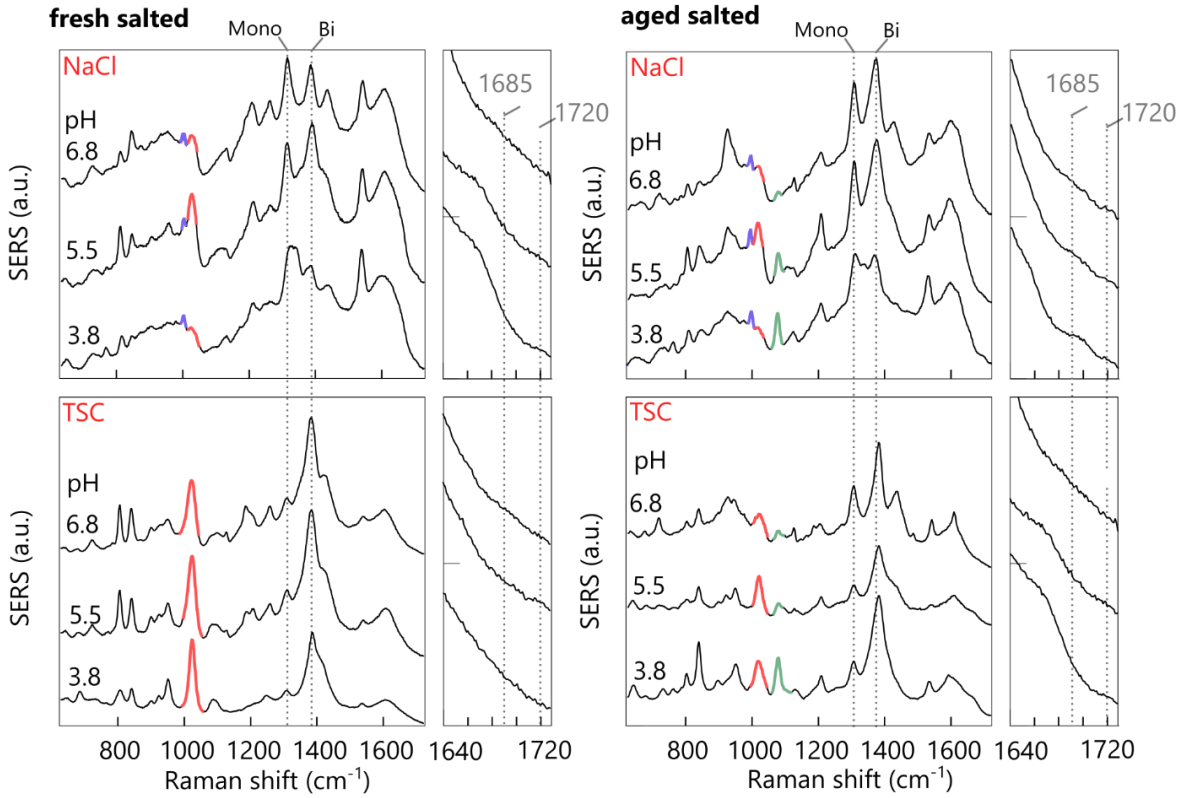

Figure S2. Salted (TSC and NaCl) AuNPs fresh *vs* aged for different pH. (a) aged and (b) salted.

For the NaCl-salted AuNPs, both fresh and aged, the 1300-1320 cm^{-1} mode indicates monodentate binding of the terminal carboxylates possibly caused by chloride ions (see main text and Figure **S13** for control measurements).

At pH=5.5, the c_2 coordination mode (1020 cm^{-1}) is more pronounced than for the lower pH=3.8 where c_2-t_2t_2 (995 cm^{-1}) dominates. This can be explained by a lower citrate surface coverage at lower pH which allows citrate ions to span the nanogap. The surface coverage is presumably lower at pH=3.8 (pKa_1=3.13) because significantly more fully protonated citrate ions exist compared to pH=5.5.

Aged NaCl AuNPs show a decrease of the adatom-driven c_2t_2-t_2 coordination with increasing pH. Conversely, a vibrational mode at 925 cm^{-1} increases with increasing pH. This mode $\nu(CCOO^-)$ of the uncoordinated central carboxylate exhibits a strong Raman activity and only occurs for t_2t_2 coordination.

The TSC salted AuNPs (~60 mM TSC concentration) show fewer coordination modes; the fresh AuNPs are clearly dominated by c_2 for all pH values. The two higher pH values contain some c_2-t_2t_2 modes as evident by the vibrations at 995 and 1535 cm^-

[1]. Aged AuNPs exhibit the adatom-driven c_2t_2-t_2. At pH=6.8, there is some indication of t_2t_2 with the emerging 925 cm^{-1}mode. A summary of the citrate coordination modes can be found in Table **S1**.

pH	fresh NaCl-salted	aged NaCl-salted	fresh TSC-salted	aged TSC-salted
3.8	c_2 **c_2-t_2t_2** c_2-t_2t_1	c_2 **c_2t_2-t_2** c_2-t_2t_2 c_2-t_2t_1 t_2t_2	**c_2**	c_2 **c_2t_2-t_2**
5.5	**c_2** c_2-t_2t_2 c_2-t_2t_1	**c_2** c_2t_2-t_2 c_2-t_2t_2 c_2-t_2t_1 t_2t_2	**c_2** c_2-t_2t_2	**c_2** c_2t_2-t_2
6.8	**c_2** **c_2-t_2t_2** c_2-t_2t_1 t_2t_2	c_2 c_2t_2-t_2 c_2-t_2t_2 c_2-t_2t_1 **t_2t_2**	**c_2** c_2-t_2t_2	**c_2** c_2t_2-t_2 t_2t_2

Table S1. Extracted citrate coordination modes for salted AuNPs. The bold-face mode is the dominant mode within the pH value. For explanation of the nomenclature, please see section three of the main text.

Arrhenius energy calculation. The adatom-induced CC-stretch at 1080 cm^{-1} observed in the CB[5]:AuNP ageing spectra (Figure **S3a**) with its linear increase over time is an excellent proxy to calculate the activation energy (Arrhenius energy) of the underlying gold adatom migration.

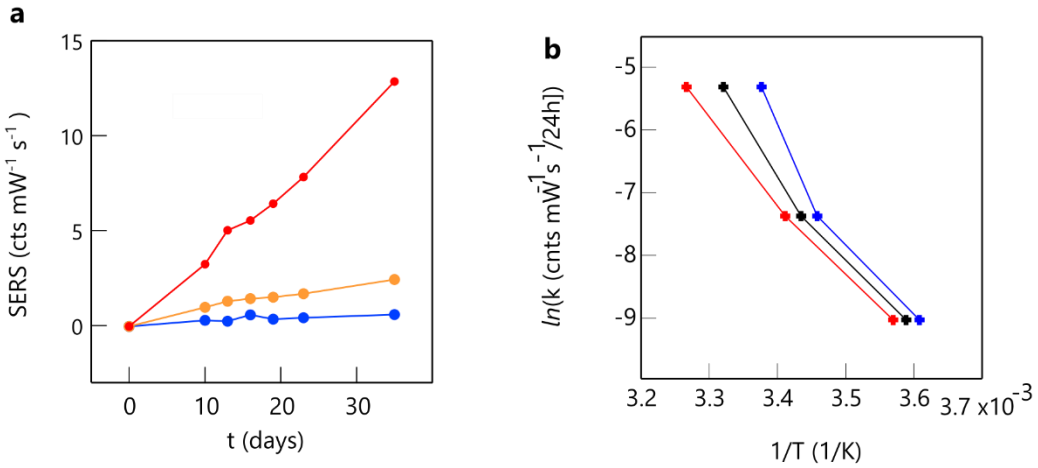

Figure S3. Activation energy of adatom mode. (a) Adatom proxy vibration for T=5, 18, 28 °C over time. (b) Extracted slopes from the peak. From the slope in (b) the activation energy can be directly extracted (see text).

For every temperature T the slope k of the CC-stretch must satisfy the equation

$$k_1 = A\, e^{-\frac{E_a}{k_B T}}$$

with k_B denoting the Boltzmann constant, A a reaction constant and E_a the activation energy. Taking the logarithm of the previous equation

$$\ln k = \ln A - \frac{E_a}{k_b}\frac{1}{T}$$

makes it possible to extract the activation energy directly from the slope m in the logarithmic plot in Figure **S5b** *via*

$$E_a = \mathrm{m}\, k_B.$$

Accounting for the uncertainty in temperature of the samples, the calculation yields an activation energy E_a= 1.1±0.2 eV = 26 kcal/mol.

Repeatability of CB[5]:AuNP. Aggregates mediated by CB[5] with a final concentration of 2.5 µM produce highly repeatable SERS signals in terms of peak intensities and SERS background (Figure **S4a**). This is due to the precise 0.9 nm gap size defined by CB[5] and the fractal morphology of the clusters.

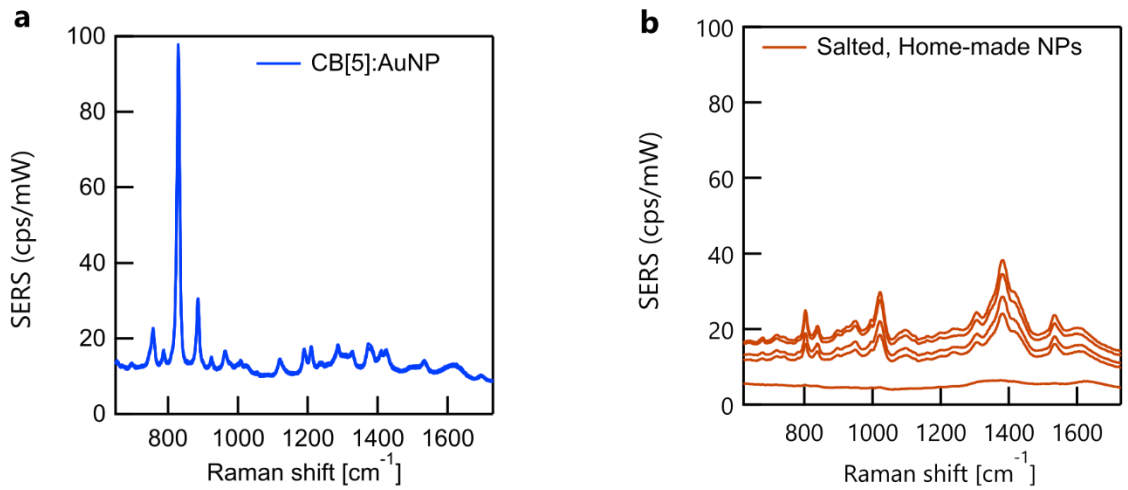

Figure S4. CB[5] *vs* salted AuNP aggregates. (a) Five slightly-aged CB[5]:AuNP samples showing high reproducibility (curves exactly superimpose). (b) Same nanoparticle stock suspension aggregated with TSC showing citrate signals and lower repeatability.

Spectra of TSC-salted aggregates of the same stock nanoparticle suspension (Figure **S4b**) are not reproducible, as evident by the varying SERS background and signal intensities. The final TSC concentration is ~60 mM.

Citrate coordination modes and DFT calculations. Coordination of the carboxylates to the Au surface results in characteristic vibrational shifts and intensity changes of the COO^- and CC stretches. This can be demonstrated by comparing the Raman response of aqueous TSC (1 M) (Figure **S5a**) to the signals of the dominant coordination mode c_2 *i.e.* bidentate with the central carboxylate (Figure **S5b**).

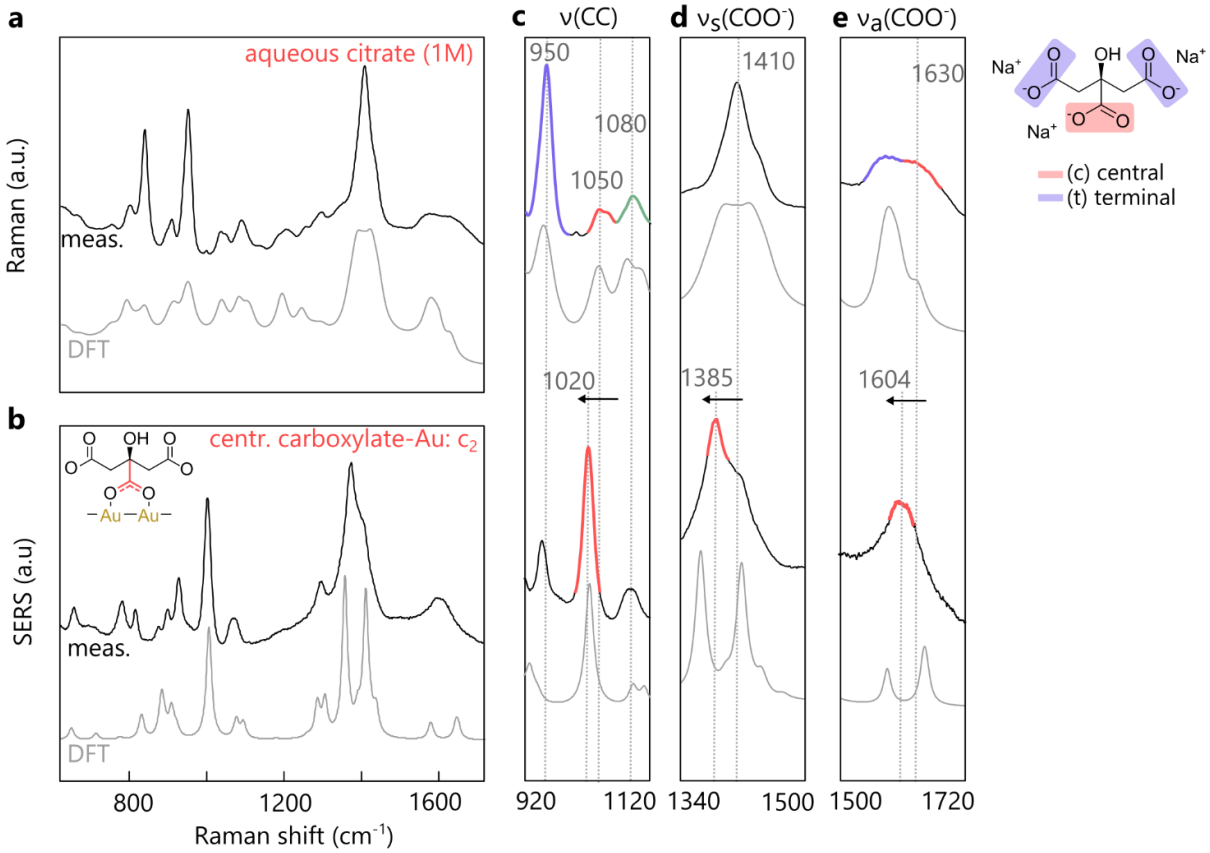

Figure S5. Aqueous *vs* adsorbed citrate. (a) Citrate chemical structure with its central (red) and terminal (blue) carboxylate. (b) Overview of carboxylate vibrations and characteristic vibrations bands depending on denticity and protonation stage, bound to Au and unbound. (c) Comparison between (top) Raman of 1M TSC *versus* SERS of TSC-salted AuNP aggregates (dominating citrate mode). (d) Carbon-carbon stretches and (e) asymmetric carboxylate stretch.

The symmetric stretch $\nu_s(COO^-)$ of aqueous citrate (Figure **S5c**, top) is located at ~1410 cm^{-1}. Upon bidentate coordination to two Au atoms (μ_2), it is blue-shifted (Figure **S7c**, bottom) to ~1385 cm^{-1}. The COO^--Au mode is not very useful for determining which of the three carboxylates are coordinated because of vibrational coupling between all three carboxylates. This makes it very difficult to disentangle each contribution. The $\nu_s(COO^-)$ stretches are good markers to distinguish between bidentate bridging (μ_2) and monodentate coordination($1\kappa:O^1$) *via* a single oxygen.

The asymmetric carboxylate stretches $\nu_a(COO^-)$ are much more suitable for distinguishing which carboxylate is bound. In aqueous citrate (Figure **S5d**, top), the COO^- stretches form a shoulder at ~1560 to 1630 cm^{-1} with a clear separation (seen in DFT) between the central (blue) and terminal carboxylates (red). Upon bidentate coordination, the vibrations are blue-shifted by ~40 cm^{-1}. Coordinated terminal carboxylates are translated to ~1530-1550 cm^{-1} and the central carboxylates (as in Figure **S5b**) to ~1560-1610 cm^{-1}. Intramolecular hydrogen bonding of the central OH-group to the bound carboxylate (as observed in DFT) has a strong influence on the position of the COO^--Au stretch. This results in an even stronger blue-shift by an additional ~20 cm^{-1}.

The carbon-carbon stretches ν(CC) of the CC bonds adjacent to the carboxylates (Figure **S7e**) exhibit very distinct shifts when their attached carboxylate coordinates to Au. The vibration of unbound terminal carboxylate is located at 950 cm^{-1} (blue), whereas the unbound central carboxylate (red) is located at 1050 cm^{-1}. Upon

coordination of a terminal carboxylate, the adjacent CC stretch is red-shifted to 960-985 cm^{-1}. The central carboxylate (Figure **S5e**) CC-stretch is blue-shifted to ~1020 cm^{-1} (strong red peak).

There are seven possible coordination modes that citrate can reach when trapped inside a nanogap (Figure **S6a**) (excluding the hexadentate mode with all three carboxylates bound to the same facet, which we find from DFT is not possible to flat Au). The distinct positions of their CC-stretches in combination with the asymmetric COO^--stretches are sufficient to distinguish these modes in a SERS spectrum.

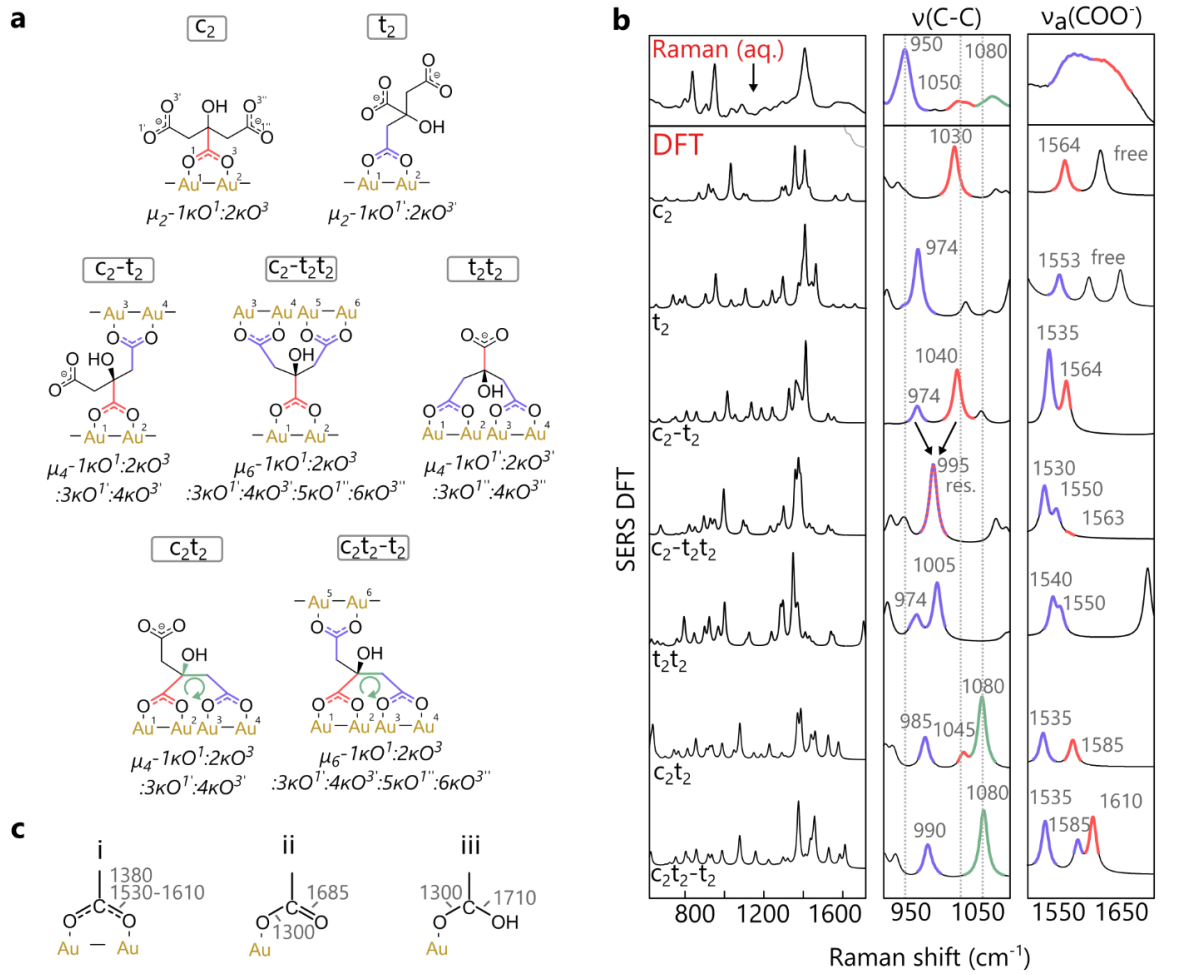

Figure S6. DFT calculations. (a) Citrate chemical structure with its central (red) and terminal (blue) carboxylate. (b) Overview of carboxylate vibrations and characteristic vibrations bands depending on denticity and protonation stage, bound to Au and unbound. (c) Comparison between (top) Raman of 1M TSC *versus* SERS of TSC-salted AuNP aggregates (dominating citrate mode). (c) Carboxylate stretches for (i) bidentate, (ii) monodentate, and (iii) monodentate (protonated carboxylate).

Compared to aqueous citrate, bidentate coordination of a terminal group (t_2) results in the red-shift of the adjacent CC stretch from ~750 cm^{-1} to 775 cm^{-1}. For the central group, the C-C stretch is blue-shifted from 1050 cm^{-1} to 1020 cm^{-1} (1030 cm^{-1} DFT).

For citrate modes with structural symmetries the central and terminal CC-stretches are coupled and can coincide to form a single vibration. This occurs in c_2-t_2t_2 (strong) and c_2t_2-t_2 (weak) resulting in a joint vibration at 990-995 cm^{-1}. This is also the case

for t_2t_2 where coupling between the two terminal groups with the unbound central carboxylate lead to a mode which is expected at ~1005 cm^{-1} (weak).

To distinguish between the triple bidentate modes c_2-t_2t_2 and c_2t_2-t_2, the CC-stretch at 1080 cm^{-1} (green) can be used. This mode becomes very active only if a terminal and the central carboxylate are bound on the same Au-facet. In measurements this mode is only observed when the terminal carboxylate coordinates to an adatom.

Apart from bidentate coordination (Figure **S6c, i**) the terminal carboxylates are also found as monodentate (**ii**) and monodentate protonated (**iii**):

- monodentate, unprotonated: the carboxylate binds with only one oxygen to a single gold atom. This leads to ν(CO) ~1300 cm^{-1} and ν(C=O) ~1685 cm^{-1},
- monodentate protonated: This leads to ν(CO) ~1300 cm^{-1} and ν(C-OH) ~1710 cm^{-1}.

As mentioned above, the central hydroxide (-OH) group of citrate prefers hydrogen-bonding to a carboxylate oxygen (intra-molecular H-bond). This affects the peak positions of the asymmetric carboxylate vibrations. The characteristic -OH···OOC bending mode is located at 1515 cm^{-1} in both measurement and DFT calculation, but only very weakly Raman active. Binding of the hydroxide group to gold (with or without cleavage of the hydrogen) is possible, but no stable geometry could be found using DFT calculations. If binding occurred *via* the –OH group, the C-OH stretching vibration (also weakly Raman active) located at 1140 cm^{-1} would undergo a shift and become much more Raman active, as is the case for the C-O-Au stretches of the carboxylate in monodentate binding.

Influence of cations (K^+, Na^+) on ageing. Concurrently to ageing experiments performed with TSC AuNPs, the same ageing protocol was applied to a batch of tripotassium citrate (TPS) AuNPs. The emerging peaks in the spectra (Figure **S7**, a-c) are identical for both cations. This suggests that the influence of cations on ageing and citrate coordination is negligible.

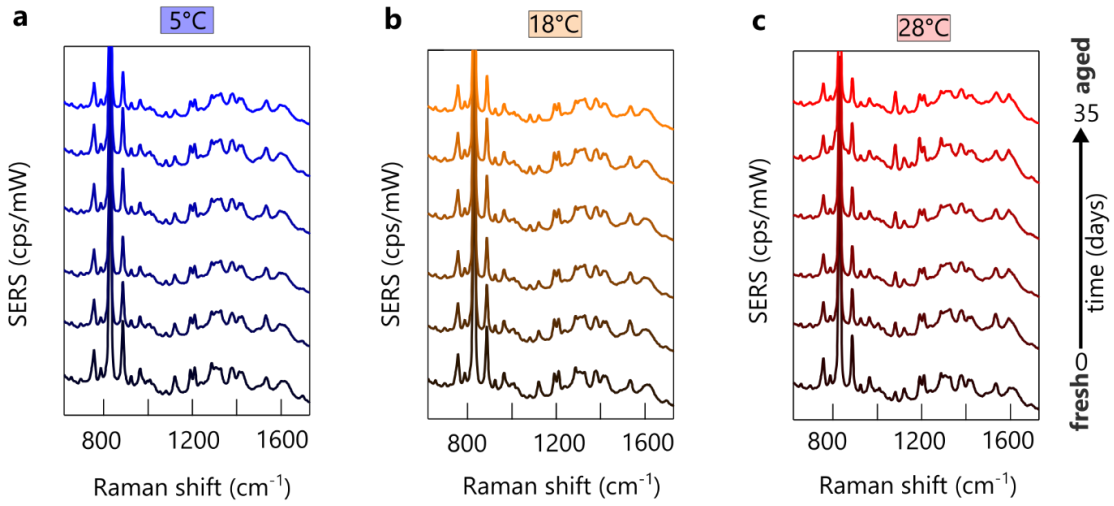

Figure S7. Ageing with K_3Citrate AuNPs. Spectra of ageing experiment for homemade TPS AuNPs stored at (a) 5 °C, (b) 18 °C, and (c) 28 °C.

Citrate decomposition products. Besides citrate, the supernatant of the AuNP suspension also contains reaction by-products (from the NP synthesis) and their thermal decomposition products. The typical decomposition pathway is: citrate, 1,3-acetone-dicarboxylate (ADC), acetoacetate (AA), and finally acetate/acetone. The unstable reaction by-products AA and ADC (both as acids and salts) undergo rapid decarboxylation during the reaction (100 °C).

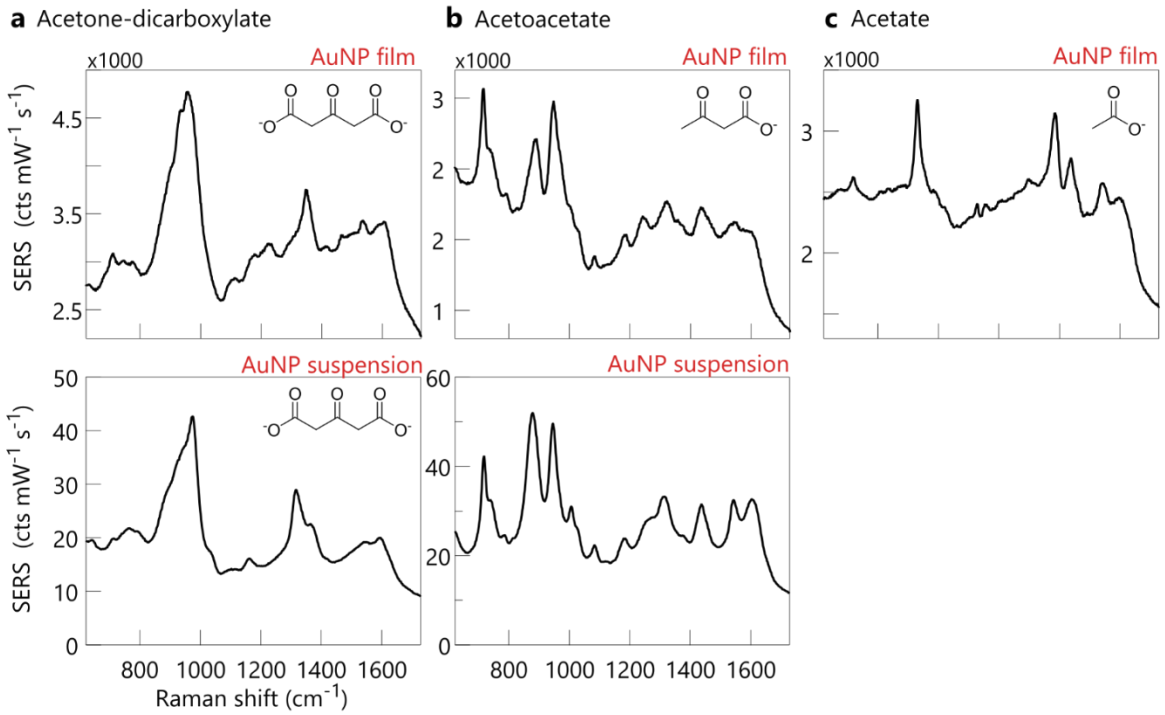

Figure S8. Spectra of decomposition products. (a) SERS spectra on AuNP film of the three most common citrate reaction by-products and their decomposition products.

Decomposition also carries on after the reaction whilst the freshly synthesised nanoparticle suspension cools down to room temperature (ca. 1h in our case).

The activation energy for the decomposition of ADC and AA are 23.9 kcal/mol=1.04 eV and 23.7 kcal/mol=1.03 eV. The rate constants at 25 °C for AA (acid) is $k = 1.64 \times 10^{-3}\ \mathrm{min}^{-1}$ and for ADC (acid) $k = 0.99 \times 10^{-3}\ \mathrm{min}^{-1}$.[1,2] Tables S2 and S3 contain the calculated decomposition times for different temperatures confirming the rapid decomposition.

acetone-dicarboxylic acid[3]		
E_a = 23.7 kcal/mole = 1.03 eV		
temperature (°C)	decomposition rate k (min^{-1})	t until 90% decomposed
5	10.3 x 10^{-5}	15 d
18	0.70 x 10^{-3}	54.6 h = 2.26 d
28	2.75 x 10^{-3}	13.9 h
100	5.93	0.39 min

Table S2. Acetone-dicarboxylic acid decomposition. Calculated decomposition rates (first order decomposition) and approximate time for 90% decomposition at different temperatures

acetoacetic acid[4]		
E_a = 23.7 kcal/mole = 1.03 eV		
temperature (Celsius)	decomposition rate k (min^{-1})	t until 90% decomposed
5	5.51×10^{-5}	29 d
18	0.38×10^{-3}	101.8 h = 4.24 d
28	1.47×10^{-3}	26 h
100	3.18	0.72 min

Table S3. Acetoacetic acid decomposition. Calculated decomposition rates (first order decomposition) and approximate time for 90% decomposition at different temperatures

Based on their SERS spectra (Figure **S8**, **a-c**) on plasma-cleaned AuNP films (top) and after the addition of excess amounts to fresh aqueous AuNPs (bottom), it is evident that observed ageing process is not related to citrate decomposition products. This is further supported by swapping the supernatant of aged and fresh AuNPs.

ADC AuNPs. It is possible to synthesise gold nanoparticles by using disodium 1,3-acetone-dicarboxylate (ADC) instead of trisodium citrate as the reducing agent. By doing so, the SERS spectra of citrate decomposition products, *e.g.* acetoacetate, without the presence of citrate can be observed.

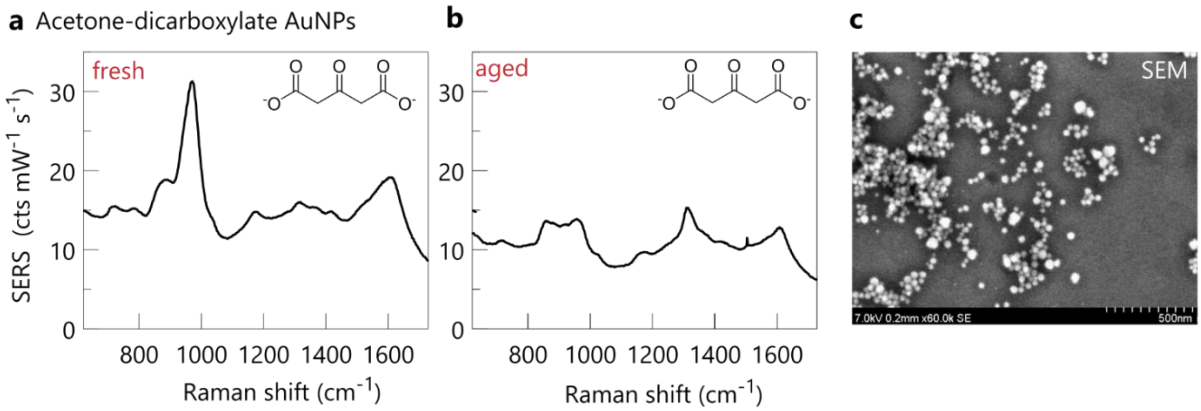

Figure S9. Disodium acetone-dicarboxylate AuNPs. (a) SERS spectrum of freshly-made NaCl-salted disodium acetone-dicarboxylate AuNPs. (b) SERS spectrum of aged NaCl-salted DAD AuNPs. (c) SEM of synthesised DAD AuNPs showing spherical particles with a "binary" size distribution.

The synthesis yields mostly spherical AuNPs with a binary size distribution (Figure **S9c**). the typical ageing response observed in citrate-reduced AuNPs is not seen even when the particles are aged (Figure **S9a**). This confirms again that thermal decomposition of citrate by-products is not responsible for ageing.

Effect of $HAuCl_4$ on AuNP size (at room temperature). Through the addition of $HAuCl_4$ to the AuNP suspension, etching of adatoms is observed. The presence of citrate also leads to a slight growth of the AuNPs. However, the reaction rate for growth is very low (it normally requires 100°C). Therefore, the balance of these two is slow etching but only of adatoms off the facets. Zeta size measurements show that the hydrodynamic radius barely increases over 2h (likely not a significant variation) (Figure **S10**).

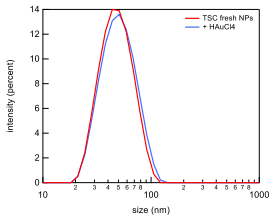

Figure S10. Etched AuNPs zeta size measurement. Slight size increase of AuNP suspension after (2h) the addition of $HauCl_4$

Control experiment: Boiling of aged AuNPs without $HAuCl_4$. Boiling aged AuNPs aggregates without addition of $HAuCl_4$ (boiled after aggregation) increases and slightly broadens the adatom mode at 1080 cm^{-1} (Figure **S11a**) This is indicative of adatoms being formed.

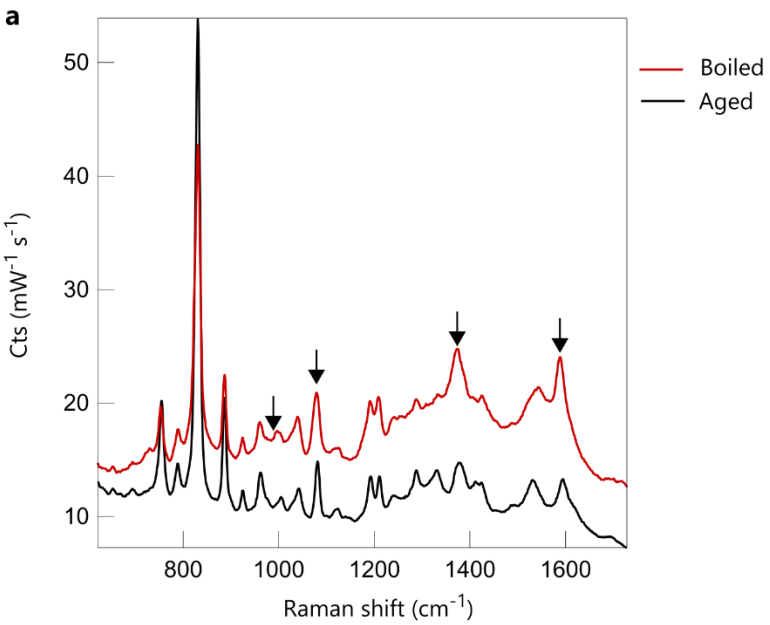

Figure S11. Boiling aged AuNP aggregates (a) Typical 'aged' CB[5]:AuNP spectrum (black) with adatom peak at 1080 cm^{-1}. Boiling of the CB[5]:AuNP aggregates leads to an increase of the adatom mode.

AuNP gap size. A geometry optimisation for citrate in the gap-spanning configuration c_2-t_2t_2 with increasing distance between the Au slabs is performed (Figure **S12a**). For an Au-Au centre distance of nearly ~1 nm, the c_2-t_2t_2 mode transitions to the non-spanning t_2t_2. This calculation gives a good intuition about the maximum gap size for the gap-spanning mode. The calculation is also consistent with what is seen in SERS measurements for fully deprotonated citrate – coordination without the central carboxylate can occur.

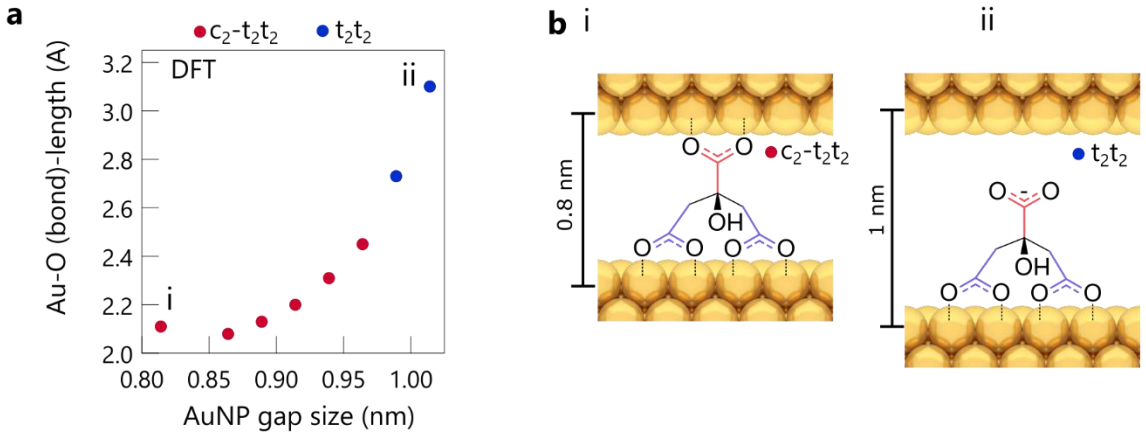

Figure S12. DFT gap size calculation. (a) Evolution of average COO-Au bond for gap size between ~0.8 nm and ~1 nm. At around 1 nm gap distance, the c_2-t_2t_2 coordination transitions into t_2t_2.

Surface chlorides and monodentate citrate binding. To prove that surface chlorides are preventing citrate from bidentate binding, AuNP aggregates are formed with a range of mono and divalent salts of which three ($MgCl_2$, $CaCl_2$, NaCl) are chlorides.

Consistent with our hypothesis, all three chloride-salted AuNP aggregates (Figure **S13a**) show the strong C-O stretch at ~1300-1320 cm^{-1} (monodentate, labelled Mono) as a result of only one carboxylate oxygen coordinated to the Au surface. Simultaneously, the decreasing intensity of the symmetric carboxylate stretch at ~1380 cm^{-1} (Bi) shows that bidentate binding is reduced. The dominant mode of the chloride-salted aggregates is clearly the gap-spanning mode c_2-t_2t_2 with the strong 995 cm^{-1} and weak 1020 cm^{-1} vibration.

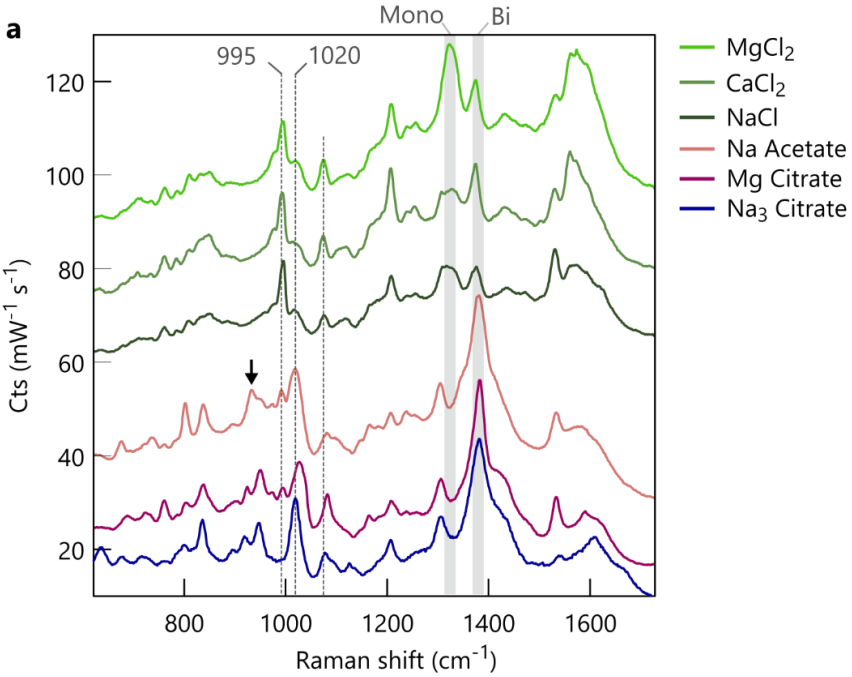

Figure S13. Chlorides in salted AuNPs. (a) Aggregation of slightly aged AuNPs with different salts. The green spectra, which all contain chloride ions, show clear evidence of monodentate

binding. Aggregation by using magnesium citrate or sodium acetate, show regular bidentate binding.

Control measurements with two citrate salts (magnesium citrate and trisodium citrate) show typical citrate signals with strong c_2 and some c_2-t_2t_2 coordination (only for Mg citrate), but no evidence of monodentate binding. The SERS spectrum for sodium acetate-salted aggregates show typical citrate signals as obtained for the citrate salts or the citrate signals on AuNP films. There is some acetate adsorbed on the Au surface (black arrow) as revealed by the characteristic ν(C-C) of acetate at 930 cm^{-1} (see Figure **S8c**). Despite acetate being adsorbed, there is no evidence of monodentate binding of the adsorbed citrate species.

Identifying surface chlorides in AuNP nano-gaps. The presence of adsorbed chlorides on the gold surface can be confirmed *via* low-wavenumber Au-Cl vibrations. Upon addition of chloride salts ($MgCl_2$, $CaCl_2$, KCl, NaCl) and also HCl to freshly aggregated AuNPs (salted with 60 mM TSC), peaks at ~170 and ~240 cm^{-1} emerge (Figure **S14**). Both peak positions are characteristic Au-Cl vibrations which have been studied in the past.[5,6]

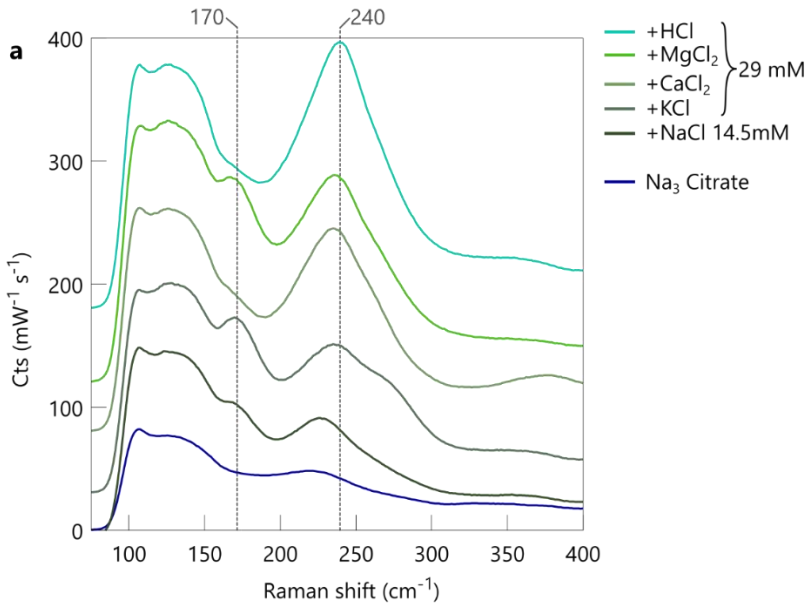

Figure S14. Trisodium citrate-salted AuNPs and chlorides. (a) AuNP aggregates formed by "salting" with TSC. After aggregation, chloride salts/HCl are added and low-wavenumber SERS is recorded. Background of spectra is shifted; no scaling is performed.

SEM close-ups of AuNP films. For the investigation of citrate binding in an environment free from citrate by-products, AuNP films are used (see methods section of main text for details). These AuNP films consist of one to three layers of close-packed 80 nm AuNPs as evident from the SEM images (Figure **S15**, **a-d**). A close-up image of the films prior to plasma treatment (Figure **S15c,** red arrows) clearly shows signs of electron irradiation damage ("halo-effect") of organic compounds deposited locally onto the AuNP surface. The O_2 plasma cleaned AuNPs with all organics removed do not exhibit this effect (Figure **S15d**). In general, it can be stated that oxygen plasma etching used here preserves the shape of the nanoparticles and their facets.

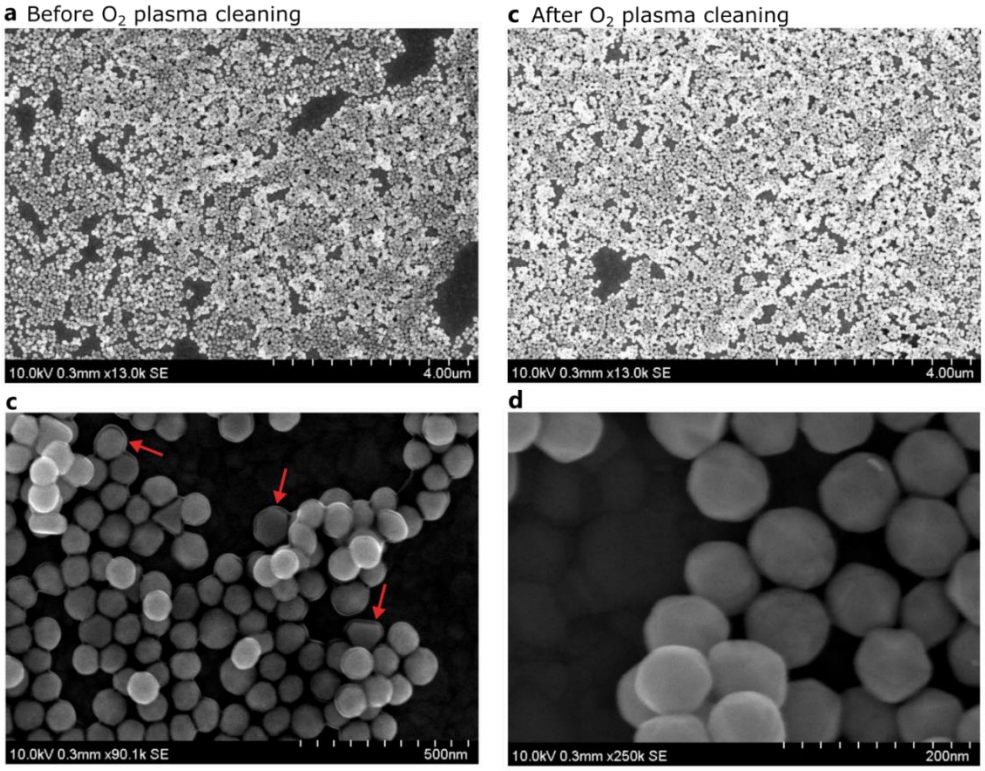

Figure S15. SEM images of AuNP films. (a,c) Films before O_2 plasma etching, while (b,d) show the films after 30 min O_2 plasma treatment. Red arrows indicate electron irradiation induced deposition of organic compounds on the AuNP surface.

Surface chlorides and monodentate citrate binding in AuNP films. Adding sodium chloride to TSC AuNP films leads to an increase in monodentate binding of citrate. Exactly the same effect is observed in colloidal gold clusters aggregated with NaCl (Figure **S16a**). The intensity of the symmetric carboxylate stretch at ~1380 cm^{-1} decreases whilst a peak at ~1300 cm^{-1} (C-O-Au stretch) emerges. Also clearly visible (black arrow) is the presence of the C=O mode of the monodentate carboxylate.

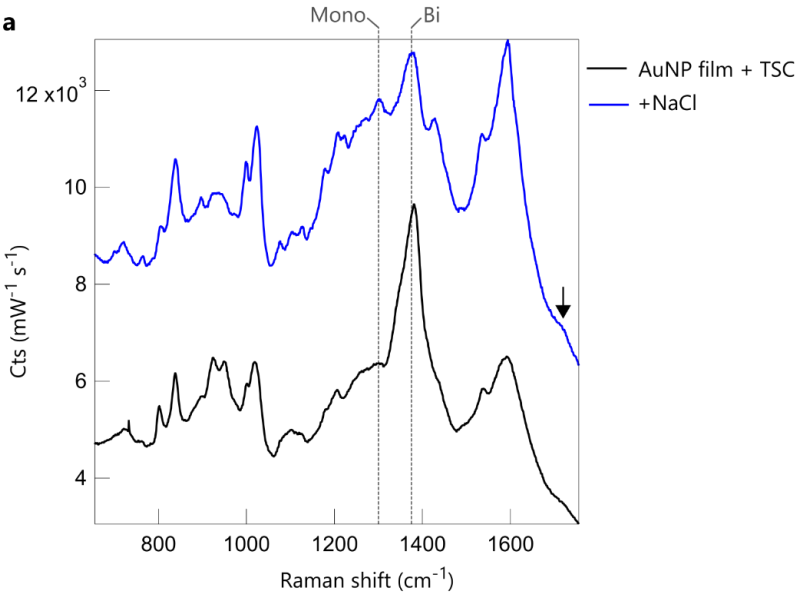

Figure S16. AuNP films with TSC and added NaCl. (a) Upon addition of NaCl (top) to a TSC sample (bottom), monodentate binding is detected.

Citrate-AuNP films ageing. To investigate the ageing behaviour of these AuNP films, a sample is kept in a citric acid solution (100 mM pH=3.5) for 87 days. The SERS spectra (Figure **S17,** a-c) show the expected c_2 coordination mode for fresh films characterised by a strong 1020 cm^{-1} vibration (red arrow). With increasing age, citrate starts to span the gaps with the modes c_2-t_2t_2 and c_2-t_2 as indicated by the 995 (dark blue) and 975 cm^{-1} (light blue) peaks. Binding of the terminal carboxylates is further confirmed by the COO^-- Au stretches at ~1530 which develop over time. For the oldest sample (87 days), a peak at 1050 cm^{-1} (black arrow) suggests the presence of uncoordinated central carboxylates. This means that also t_2 modes are present. As discussed in the main text, the lack of the 1080 cm^{-1} vibrations suggests that the underlying ageing pathway of AuNP films is different to the colloidal case.

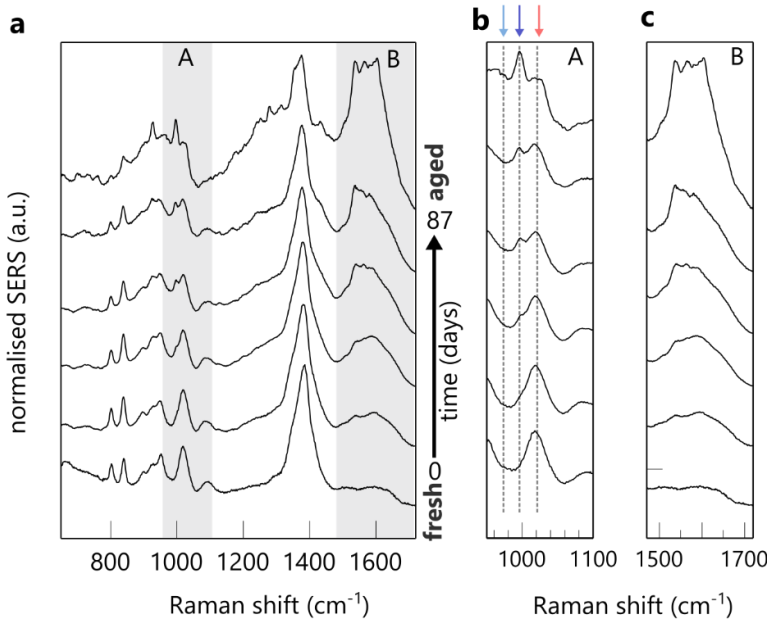

Figure S17. Ageing of AuNP films. (a) Ageing spectra, with (b) CC-stretches, (c) asymmetric COO^-- Au stretches. Arrows: Light-blue marks 785 cm^{-1} vibration, dark blue 995 cm^{-1} and red 1020 cm^{-1}.

References

(1) Yasuda, M. Dissociation Constants of Some Carboxylic Acids in Mixed Aqueous Solvents. *Bull. Chem. Soc. Jpn.* **1959**, *32*, 429–432.

(2) Doyen, M.; Bartik, K.; Bruylants, G. Journal of Colloid and Interface Science UV – Vis and NMR Study of the Formation of Gold Nanoparticles by Citrate Reduction : Observation of Gold – Citrate Aggregates. *J. Colloid Interface Sci.* **2013**, *399*, 1–5.

(3) Larson, D. W.; Lister, M. W. Catalytic Decomposition of Acetonedicarboxylic Acid. *Can. J. Chem.* **1968**, *46*, 823–832.

(4) Hay, B. R. W.; Bond, M. A. Kinetics of the Decarboxylation of Acetoacetic Acid. *Aust. J. Chem.* **1967**, *20*, 1823–1828.

(5) Gao, P.; Weaver, M. J. Metal-Adsorbate Vibrational Frequencies as a Probe of Surface Bonding: Halides and Pseudohalides at Gold Electrodes. *J. Phys. Chem.* **1986**, *90*, 4057–4063.

(6) Chan, M. Y.; Leng, W.; Vikesland, P. J. Surface-Enhanced Raman Spectroscopy Characterization of Salt-Induced Aggregation of Gold Nanoparticles. *ChemPhysChem* **2018**, *19*, 24–28.